Flexible and Printed Electronics

PAPER

Study of inkjet-printed serpentine structure on flexible substrates deformed over sculptured surfaces

Isaac A Bower , Christine L Taylor and Suresh K Sitaraman

The George W. Woodruff School of Mechanical Engineering, Georgia Institute of Technology, Atlanta, GA 30332, United States of America

E-mail: suresh.sitaraman@me.gatech.edu

RECEIVED
14 September 2019

REVISED
14 December 2019

ACCEPTED FOR PUBLICATION
2 January 2020

PUBLISHED
26 February 2020

Keywords: inkjet printing, silver ink, conductivity, microstructure, polymer substrates, bend test, finite element analysis

Abstract

The electrical resistance of inkjet-printed silver structures on polymer substrates deformed over complex sculptured surfaces is studied in this work. Mating sculptured surfaces with complex surfaces are designed and fabricated using 3D additive printing of plastic materials. These sculptured fixtures are fabricated to be able to be fit onto a universal test machine. Two types of surfaces are considered in this study: (1) biaxial or dome-shaped bending to produce bi-axial tension on the printed elements and (2) convex/concave saddle-like bending to produce bi-axial tension and compression on the printed elements. Conductors are fabricated on two polymer substrates: polyethylene terephthalate (PET) and liquid crystal polymer. Electrical resistance of the printed conductors is measured prior to deformation, as well as while being subjected to multi-directional deformation in the sculptured fixtures. Both monotonic as well as fatigue experiments have been carried out. Numerical simulations are carried out to determine strain distribution in the flexible structure as it is being subjected to these multi-directional deformations. Strain results from these simulations are compared with hand calculations and experimental data.

1. Introduction

Flexible electronics is an emerging field with an immense amount of applications such as human health monitoring [1, 2], communications [3, 4], wearable and smart fabrics [5, 6], and others Being able to be bent, stretched, twisted, folded, and conformed to surfaces are attractive properties for flexible electronics. These properties provide ease of use, durability, comfort, and adaptability.

Recently, there is increased interest in printed electronics on flexible substrates to facilitate various stretching, bending, twisting, and folding operations. These printing methods are used to apply various materials such as conductors [7] and dielectrics [5]. Popular printing methods include inkjet, aerosol, screen, gravure, and flexographic printing.

Each of the different printing techniques has its own set of advantages and disadvantages. For example, gravure and flexographic printing are good for large production but has expensive initial tooling setups. Inkjet printing is initially cheaper, but has issues with thermal compatibility of substrates with curing processes required by the inks. Aerosol jet printing can produce fine features, but is slow. Screen printing is cost effective and easy to use, but has feature size limitations. Micro-dispense printing allows the dispensing of very viscous inks, but also has feature size limitations. The ideal printing method depends on many factors such as feature size, number of samples, type of substrate etc.

Polymer substrate materials commonly used include polyimide (PI), polyethylene terephthalate (PET), polyethylene naphthalate (PEN), thermoplastic polyurethane (TPU), and liquid crystal polymer (LCP). Polyimide is commonly used due to its ability to withstand very high temperatures [8] which are needed for many inks used in inkjet and aerosol jet printing. PET is cheaper, but it cannot withstand as high of temperatures [9]. TPU is a hyperelastic material and works well in applications where stretchability is essential. However, TPU also cannot handle high temperatures. LCP is a good choice for high speed applications due to its low loss and low moisture absorption [10], but has limited flexibility and stretchability.

There are many different categories of flexible electronics that are fabricated by printing. These include

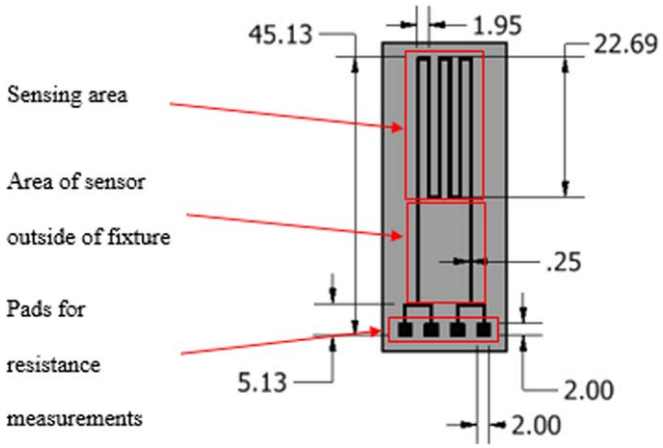

Figure 1. Serpentine pattern design (dimensions in mm).

Table 1. Summary of printed samples.

Sample set	Printer	Substrate	Ink	Sintering
1	Epson® Stylus® C88+	Novele™ IJ-220 PET	Novacentrix® Metalon® JS-B25P ink	Air-dried
2	Epson® Stylus® C88+	Novele™ IJ-220 PET	Novacentrix® Metalon® JS-B25P ink	Oven 90 °C for 30 min
3	Dimatix™ 2831	Rogers Ultralam® 3850HT LCP	Sun Chemical® Suntronic™ EMD 5730 ink	Oven 200 °C for 30 min

antennas [3, 4], conductors, inductors, sensors, capacitors [5, 11], batteries [12, 13], and many others. This paper will be focusing specifically on inkjet-printed serpentine structures.

Because these electronics are made with the intent of being deformed, work needs to be done to understand how their performance changes when stretched, bent, twisted, or otherwise deformed. Most tests that are conducted focus on stretching [14–16] or uniaxial bending [17–19]. There is also an ASTM testing standard for uniaxial mandrel bending of printed electronics [20]. Even though these tests provide useful information about the performance of these electronics, the flexible electronic systems undergo multiaxial deformation in actual applications. Because of this, tests need to be developed to understand the performance and reliability of these devices and their materials on such multiaxial surfaces. In this work, a test is developed for conforming flexible printed electronics to multiaxial surfaces such as a dome or a saddle shape. This test is then used to test the performance or inkjet-printed serpentine patterns on flexible polymer substrates to understand the behavior of their materials under this type of cyclic loading.

2. Surface deformation testing

2.1. Fabrication

Test samples were fabricated by inkjet printing silver nanoparticle ink on flexible polymer substrates. The inks used contained silver nanoparticles suspended in a fluid that evaporates off to leave a structure of fused particles. The geometry of the printed structures is a serpentine structure with pads for four-point measurements. The samples were designed to fit onto the fixtures made to apply the deformation. Figure 1 shows the dimensions and different areas of the serpentine pattern design.

Three different sets of serpentine patterns were printed. The first two sets were printed on PET while the third set was printed onto LCP. The first two sets were printed using an Epson® C88 + regular desktop inkjet printer where spare cartridges were filled with Novacentrix® Metalon® JS-B25P silver nanoparticle ink. This ink was deposited on Novele™ IJ-220, a microporous coated PET. One set was allowed to dry at room temperature while the second set was sintered in an oven at 90 °C for 30 min. One layer of ink was printed for these two sets. The third set of samples was fabricated by printing Sun Chemical® Suntronic™ EMD 5730 silver nanoparticle ink using a Dimatix™ 2831 inkjet printer. The ink was printed onto Rogers Ultralam® 3850HT LCP and sintered in an oven at 200 °C for 30 min. Four layers of ink were printed in the same locations to create a thick ink layer. Table 1 gives a summary of the three sets of samples with their materials and fabrication details.

Figures 2 and 3 show examples of an oven-sintered PET and LCP serpentine structure.

Resistance values of five samples of each set are shown in table 2.

One can see that the resistance of the oven-sintered PET samples were about half of that of the air-dried PET samples. When the Novacentrix® ink is printed onto the microporous coating on the PET, the capping

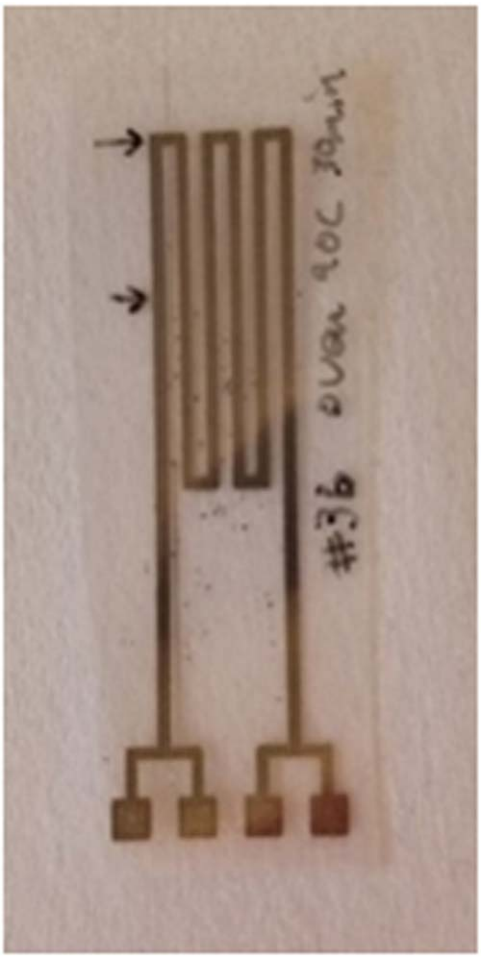

Figure 2. Serpentine pattern made with Novacentrix® Metalon® JS-B25P ink on Novele™ IJ-220 PET.

Figure 3. Serpentine pattern made with Sun Chemical® Suntronic™ EMD 5730 ink on Rogers Ultralam® 3850HT LCP.

layer on the silver nanoparticles is moved off creating contact between the particles and electrical conductivity. When the sample is cured in the oven, the capping layer is further removed creating even better contact between particles and lower resistivity. This phenomenon, along with any densification of the material while in the oven is why the resistance is so much lower for the oven-sintered PET samples than the air-dried PET samples. The resistance of the patterns on LCP was significantly lower than the resistance of the patterns on PET. This is most likely a combination of higher print quality from using a Dimatix™ printer which is commonly used for printing electronics as opposed to a modified standard desktop inkjet printer, and also due to the higher temperature used in the sintering process. The different ink formulations will also have an effect on the final properties. The thickness of the Novacentrix® was assumed to be quite low due to the ink being printed on a microporous coating. The printed Suntronic™ ink was assumed to be about 8 μm thick based on previous experience with this same ink.

2.2. Sculptured surfaces

Two sculptured surfaces were explored—dome shape having a biaxial radius of 101.6 mm (4 in.) and a saddle shape with a concave radius of 101.6 mm and a convex radius of 101.6 mm. The shapes were designed in Autodesk® Inventor and 3D printed PLA in Ultimaker 2+. Figure 4 shows the two surfaces.

Figure 5 shows test fixtures designed with these two surfaces. Mounting areas were designed into the fixtures to enable mounting to a Test Resources™ 100 universal test machine (UTM).

Figure 6 shows 3D-printed saddle and dome test fixtures.

Table 2. Initial resistance results.

Sample	Resistance (Ω) Air-dried on PET	Resistance (Ω) Oven-sintered on PET	Resistance (Ω) Oven-sintered on LCP
1	302.6	167.0	19.55
2	301.6	167.3	30.91
3	377.2	128.5	21.88
4	299.8	135.7	26.37
5	309.2	146.0	24.06
Average	314.7	148.9	24.55

2.3. Test setup and execution

Fixtures were attached to the UTM as shown in figure 7.

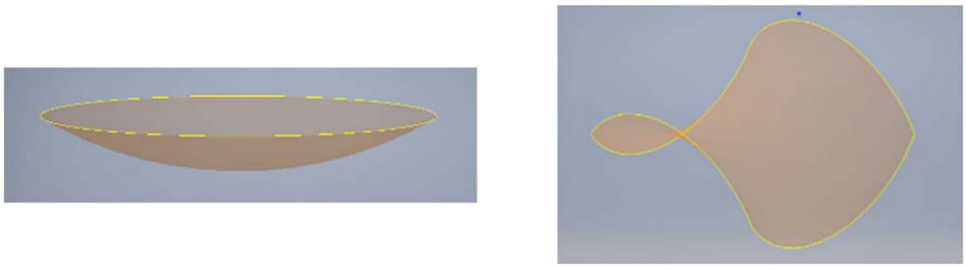

Figure 4. CAD models of surfaces explored: 101.6 mm dome (left) and 101.6 mm saddle-like (right).

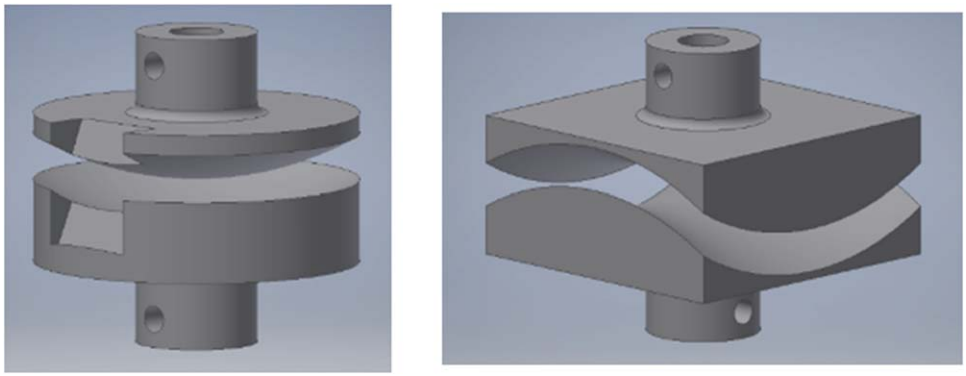

Figure 5. CAD models of dome (left) and saddle-like (right) fixtures designed to fit onto UTM.

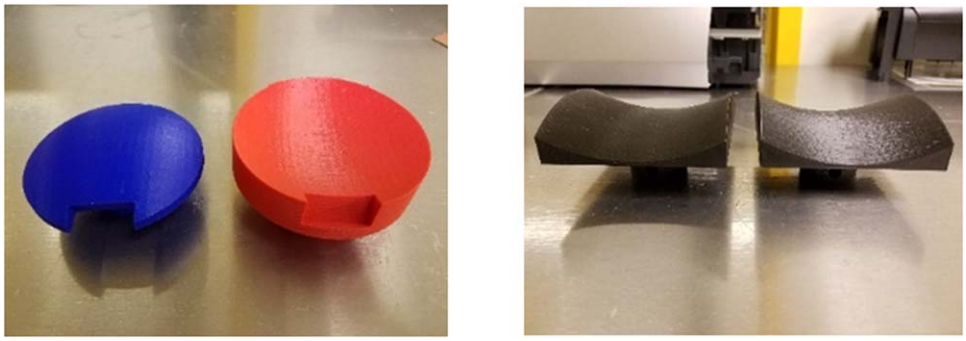

Figure 6. 3D printed test fixtures: dome (left) and saddle-like (right) fixtures.

A pogo pin fixture was fabricated in order to facilitate easy measurements of the printed pattern during testing. This fixture consisted of four pogo pins glued into a top piece and a bottom piece with a flat surface. Screws were placed in two outer holes on the top piece and screwed into threaded holes on the bottom piece. The sample was placed in between the two pieces and the screws were tightened. As the screws were threaded through the bottom piece, the pogo pins clamped down onto the contact pads. Figure 8 shows a printed LCP sample with the pogo pin fixture attached.

Soft wipes were placed under and on top of the sample to prevent the fixtures from scraping the sample. Figure 9 shows the sample with the pogo pin connector placed in the dome fixtures.

The sample with the pogo pin connector was first placed on the bottom fixture and held in place with a tape. The top fixture was at a sufficient distance away from the bottom fixture without any contact with the sample. The four-point resistance measurements were started and taken every 0.5 s with a probe current of 100 mA. The top fixture was then given a downward displacement of 20 mm min^{-1}, and the load and the resistance of the serpentine structure were continuously monitored. The displacement continued until there was a load high enough to show that the sample was fully clamped (around 100 N depending on which fixtures and substrate materials were being used). When this load reading was reached, the downward movement was stopped and the sample was held

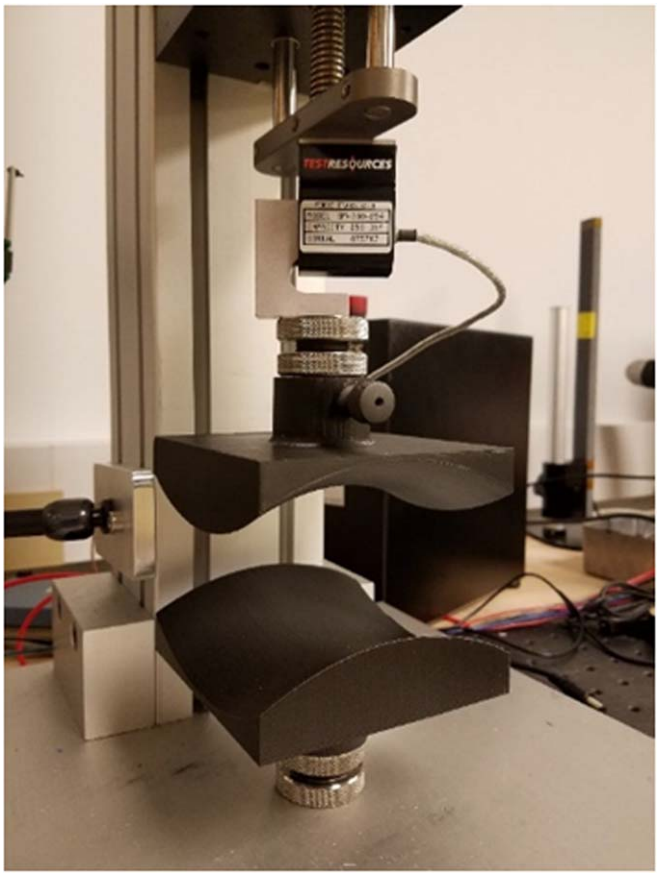

Figure 7. Test Resources™ UTM with saddle fixtures attached.

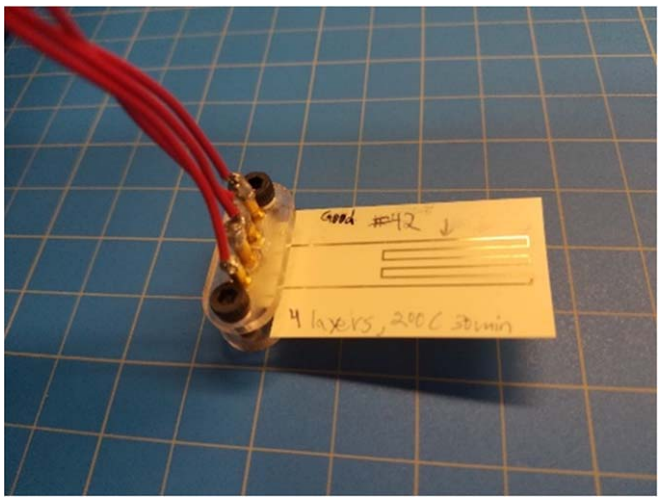

Figure 8. LCP sample with pogo pin connector attached.

fully clamped for 10 s. This is the loading part of the experiment. The top fixture was then given an upward displacement of 20 mm min^{-1} to unload the sample. This upward movement was continued for 45 s so that the top fixture was far away at a place where it was no longer touching the sample. The downward movement, the hold, and the upward movement for a total 100 s completed one cycle. Tests were conducted for 100 to 300 cycles.

The serpentine patterns tested were oriented where the ink structures were under bi-axial tension during the dome tests. On the other hand, the ink structures were under tension in the length direction and compression in the width direction during the saddle-like

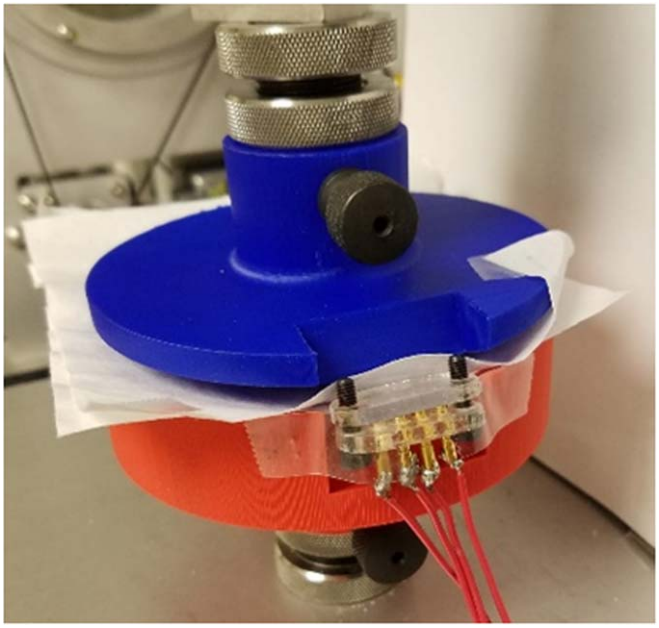

Figure 9. Sample in dome fixtures.

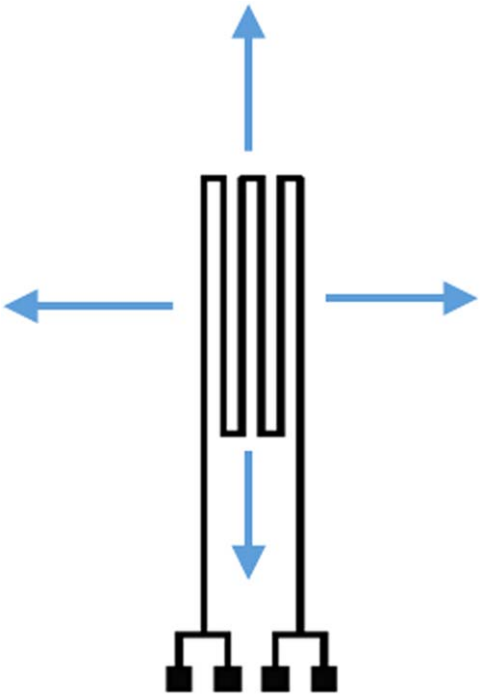

Figure 10. Tension directions during dome test.

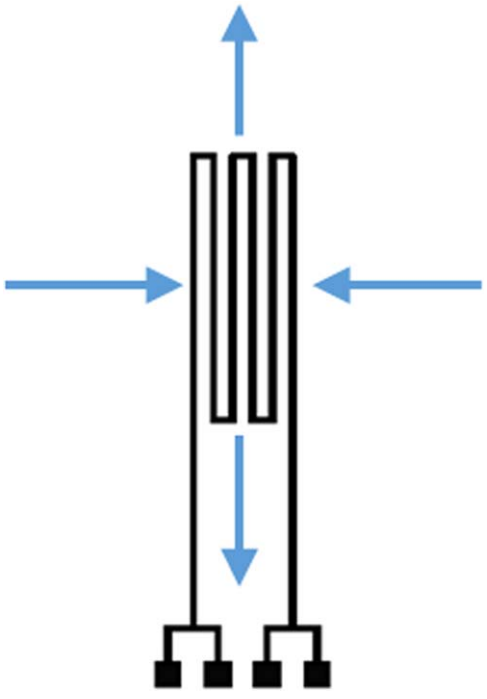

Figure 11. Tension and compression directions during saddle-like surface test.

tests. Figures 10 and 11 show the tension and compression directions on the serpentine geometry.

2.4. Testing of air-dried PET samples

First, the air-dried PET samples with Suntronic™ ink were tested on the dome. Figures 12 and 13 show the resistance data of one of the tests using-air-dried ink.

In figure 13, the flatter area before and after the bump represent the time where the sample was not under any load. The increase in resistance represents the time when the sample starts to be loaded, the flat area with higher resistance represents the 10 s where the sample is fully clamped, and the area with sharp decreasing resistance represents the sample being unloaded. One can see from figure 13 that the change in resistance is about 0.1%. It should be pointed out that although the resistance increased during loading in each cycle, the overall resistance showed a continued decrease in resistance with cycling. This phenomenon

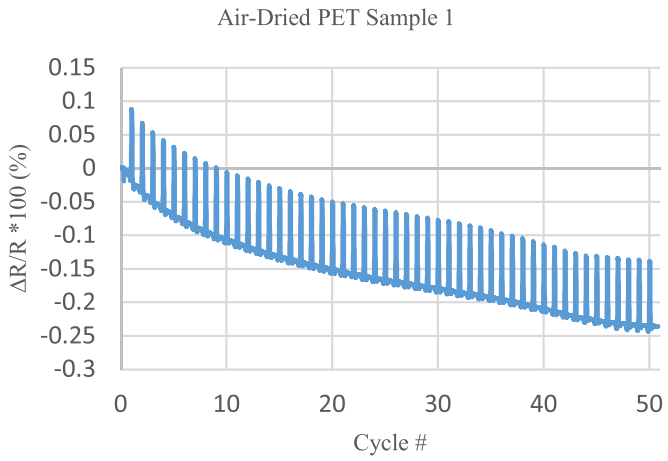

Figure 12. Resistance data of air-dried PET sample 1 during dome test.

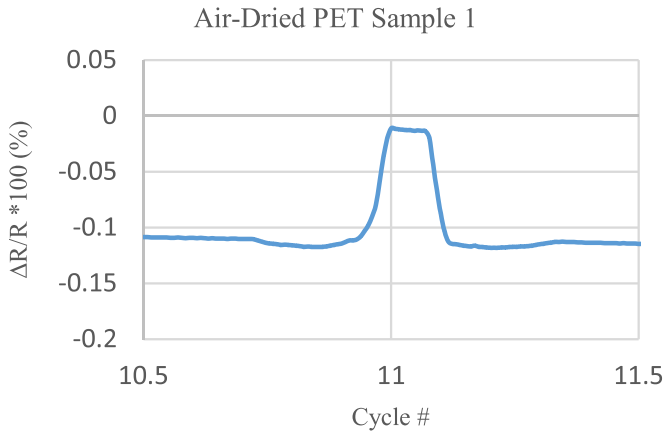

Figure 13. Close-up resistance data of air-dried PET sample 1 during dome test.

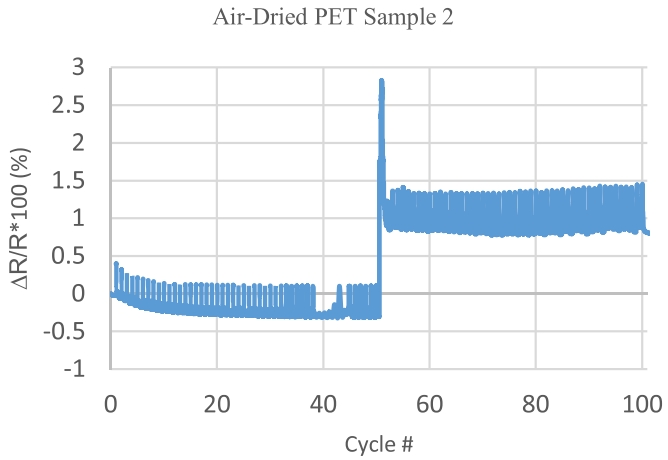

Figure 14. Results of air-dried PET sample 2 during dome test.

has been seen in the same ink in other yet-to-be-published research by other collaborating researchers elsewhere. Additional discussion on this phenomenon is presented in a later section in this chapter.

Figure 14 shows another air-dried PET sample subjected to a dome test. The gap in the resistance band from about 38 cycles to about 45 cycles is due to an accidental programming change in data sampling rate, and

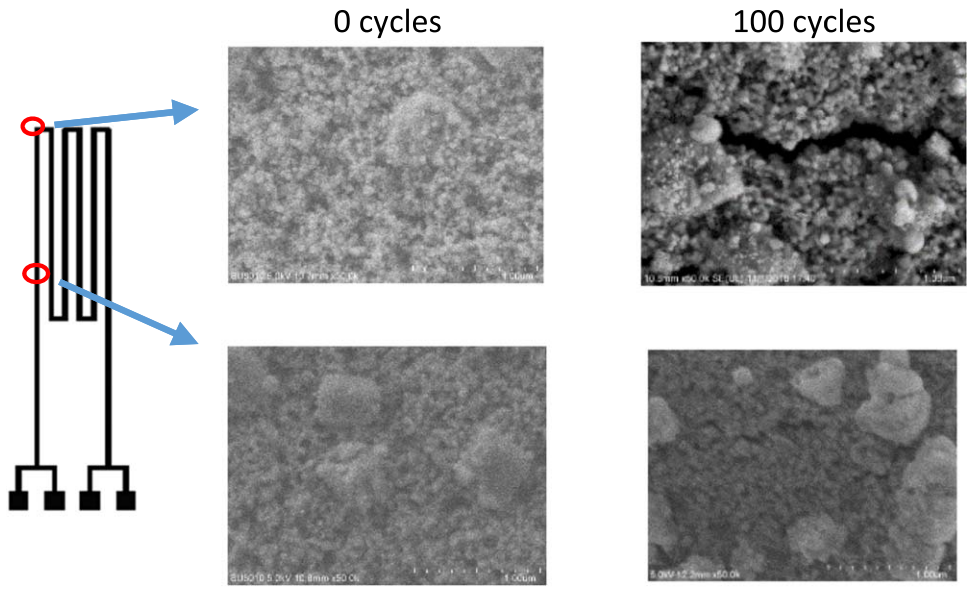

Figure 15. SEM images of second air-dried ink on PET sample at zero and 100 cycles taken at 50 k magnification.

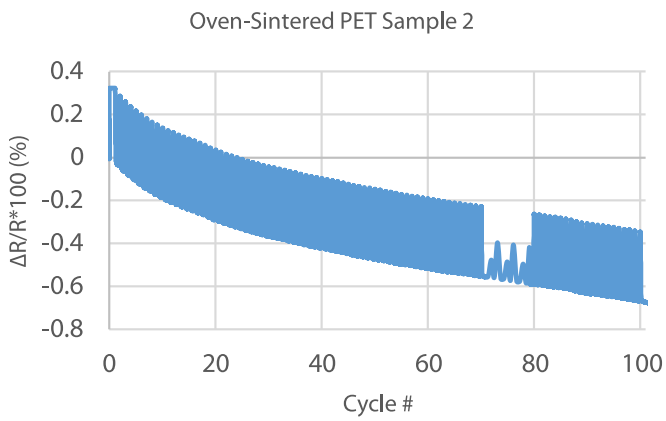

Figure 16. Results of all 100 cycles of oven-sintered PET sample 2 during dome test.

is not related to any real resistance change or failure in the sample. As seen, the resistance suddenly increases after 50 cycles and stays higher thereafter. This is due to cracking of the ink from fatigue loading, as shown later in scanning electron microscopy (SEM) images.

Figure 15 shows the locations of SEM imaging and these images of the second air-dried PET sample at zero and 100 cycles.

2.5. Testing of oven-sintered PET samples

Dome tests were performed on PET samples sintered in the oven as well. Figure 16 below shows the resistance results of an oven-sintered PET sample subjected to a dome test. The gap in the resistance band from about cycle 70–80 is due to a change in sampling rate similar to that seen in figure 14.

As seen, with oven-sintered samples on PET, the overall resistance continues to drop cycling, as happened in air-dried samples. However, with the oven-sintered samples, the resistance does not show any sudden increase after 50 cycles, unlike the air-dried sample on PET. This indicates that there is possibly no cracking in the ink over 100 cycles. This is also demonstrated through SEM images as shown in figure 17.

2.6. Testing of oven-sintered LCP samples

Before discussing the test results for samples on LCP, it may be worthwhile to re-state some of the processing conditions. The serpentine patterns were made with Suntronic® ink ink-jet printed on Rogers LCP and sintered at 200 °C for 30 min.

The LCP samples were tested in a similar way as the PET samples. One of the LCP samples was tested on the saddle for 300 cycles with the length of the serpentine pattern in tension. SEM imaging was taken at

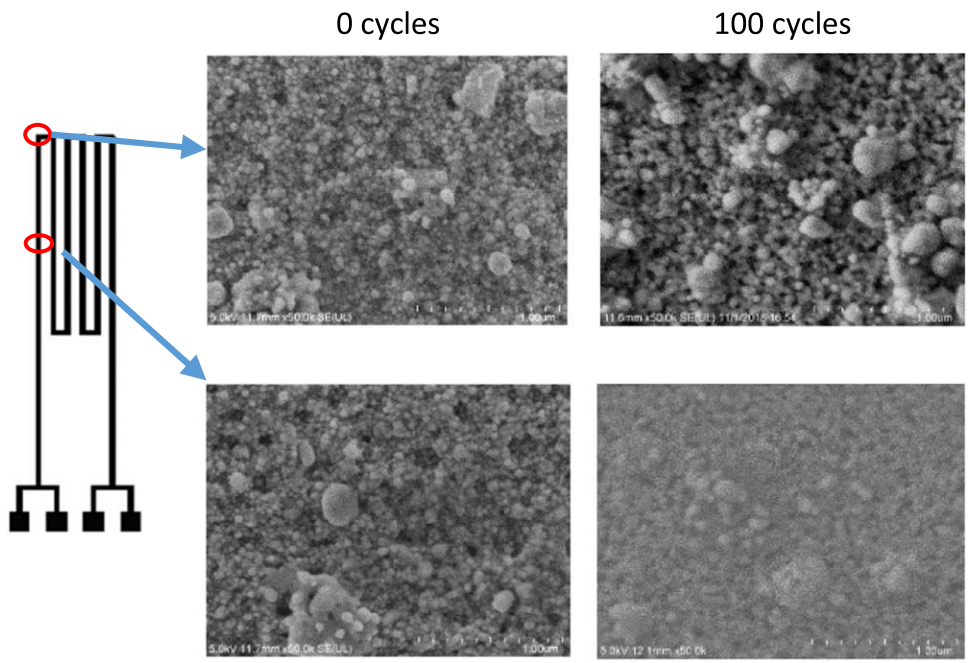

Figure 17. SEM images of 2nd oven-sintered PET sample at zero and 100 cycles taken at 50 k magnification.

0, 100, 200, 250, and 300 cycles in the same way as the PET samples. Cracks were first seen in the corner location at 200 cycles, and at the side location at 250 cycles. Figure 18 shows SEM images taken at the corner and side locations at 0, 200, 250, and 300 cycles.

Figure 19 shows resistance values just after 100 cycles.

Figure 20 shows resistance values just after 250 cycles.

The resistance continued to increase and the cracks continued to grow. Figure 21 shows the resistance results for this sample at the end of the test.

As expected, the resistance kept increasing over time with a total increase of over 20%. The SEM images from the areas in the middle of the trace showed cracks developing in the horizontal direction, while those in the corner showed cracks developing at large angles. In addition, the cracks appeared earlier in the corner location and were larger. There does not appear to be any individual particles splitting apart, and the cracks were inter-particle, rather than intra-particle.

2.7. Results and discussion

The major differences between the different printed silver inks are their particle distributions and the fusing of the particles during curing. One can see from figure 17 that the Novacentrix® ink has a fairly large distribution of particle sizes from small to large pieces. In addition, the particles in this ink do not appear to undergo significant fusing during the oven curing. The images at the top left of figure 18, (0 cycles), show the structure of the Suntronic® ink after curing in the oven, but before it had undergone mechanical cycling. These images show that the particle distribution in the Suntronic® ink is more uniform than that of the Novacentrix® ink. Also, unlike the Novacentrix® ink, the Suntronic® ink undergoes significant fusing during the curing process. The most likely reason for this is the difference between curing temperatures (200 °C versus 90 °C). One interesting observation is the difference between the ink structures of the oven-sintered and air-dried Novacentrix® ink. One can see from figures 15 and 17 that there does not appear to be a significant difference. Even though there is not much of a visual difference, the oven-sintered samples did have a much lower electrical resistance. One possible reason is that the capping agent within the ink flows off the particles better at higher temperatures or the elevated temperature causes it to decompose.

The resistance trends during cycling for the Novacentrix® ink on PET samples requires additional discussion. One would expect the resistance of the silver ink to immediately increase during cycling as the ink structure is damaged. The resistance of both the oven-sintered and air-dried Novacentrix® samples decreased during each test. As the cycling continued, the resistance trend would either start to flatten out or begin to increase. This goes against what is usually seen in literature when silver inks undergo cyclic straining. There have been observed cases of thin metal films deposited by evaporation on polymers whose electrical resistance decrease during cyclic loading [21, 22]. This, however, was not seen in the silver ink tests performed alongside these films [22]. The decrease in resistance in the Novacentrix® ink samples most likely has something to do with the microporous coating on PET substrates onto which the ink was printed. It is hypothesized that with repetitive loading and

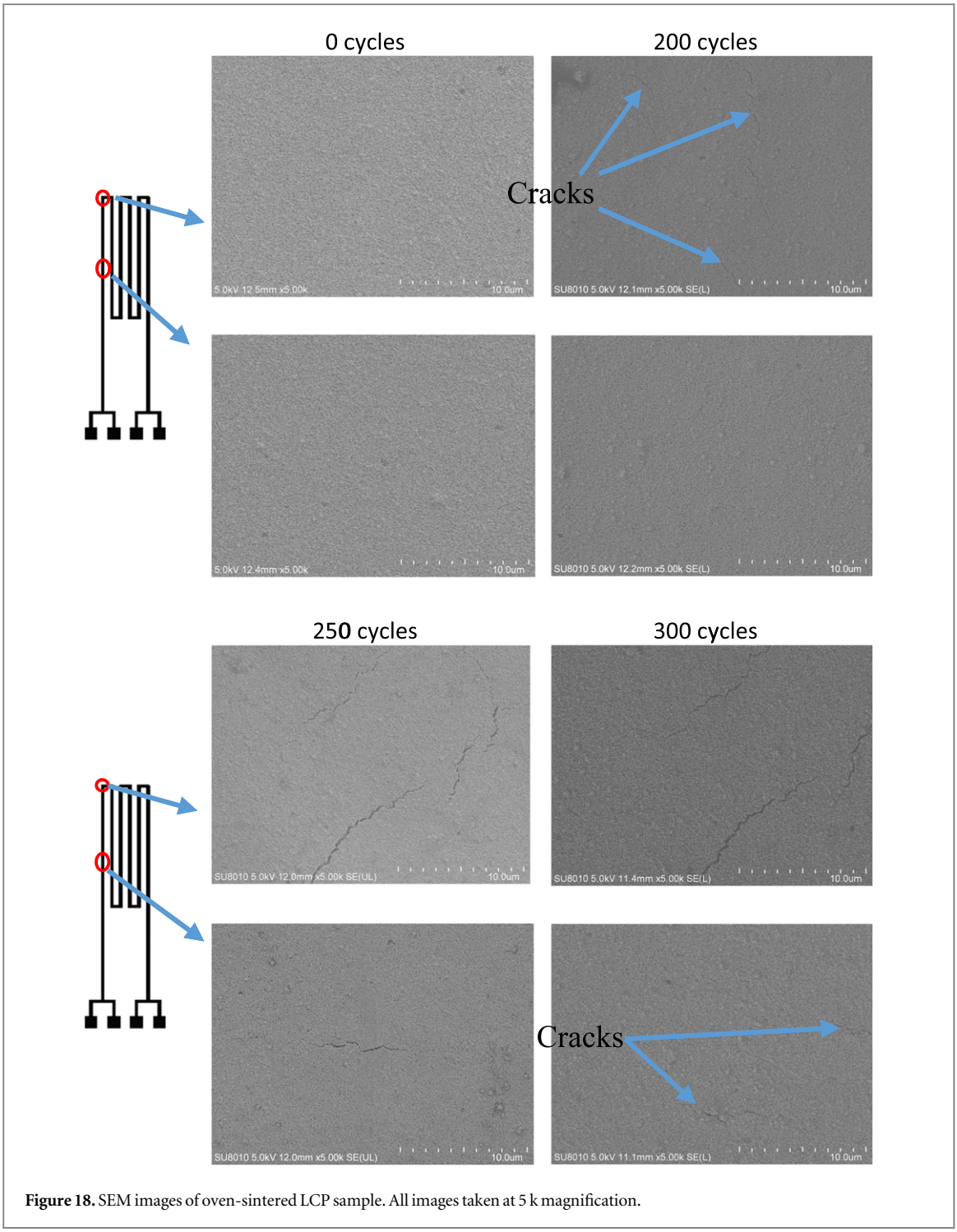

Figure 18. SEM images of oven-sintered LCP sample. All images taken at 5 k magnification.

unloading cycles, the capping layer on the particle break and thus, particle-to-particle contact improves resulting in lower resistance with fatigue cycling.

3. Modeling

Simulations of the dome and saddle-like loading conditions were conducted for the printed serpentine geometry. For the simulations, only the Suntronic™ ink printed on LCP geometry was examined. The geometry was modeled in Autodesk® Inventor and the simulations were performed using ANSYS® Workbench 17.1.

3.1. Material modeling

The material combination chosen was the Suntronic™ ink printed on LCP substrate. Isotropic elastic material models were used in the simulations. A modulus of 13.5 GPa was used for the silver ink from previous nanoindentation experiments. Poisson's ratio was assumed to be the same as bulk silver at 0.37. The LCP material properties were taken from the product's datasheet [8, 23]. The fixtures were modelled as

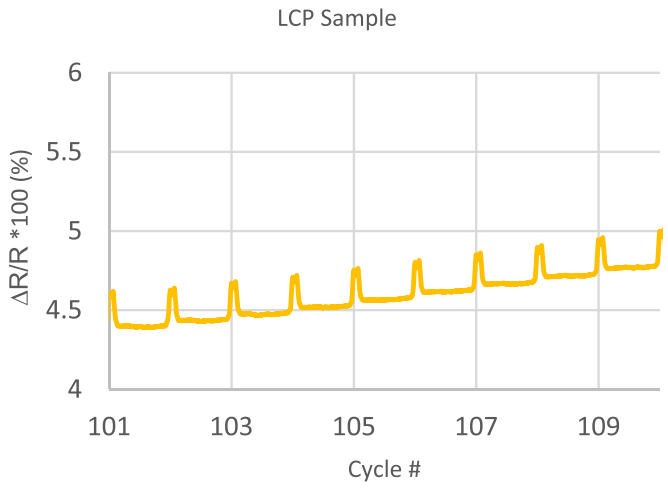

Figure 19. Resistance results of LCP sample just after 100 cycles.

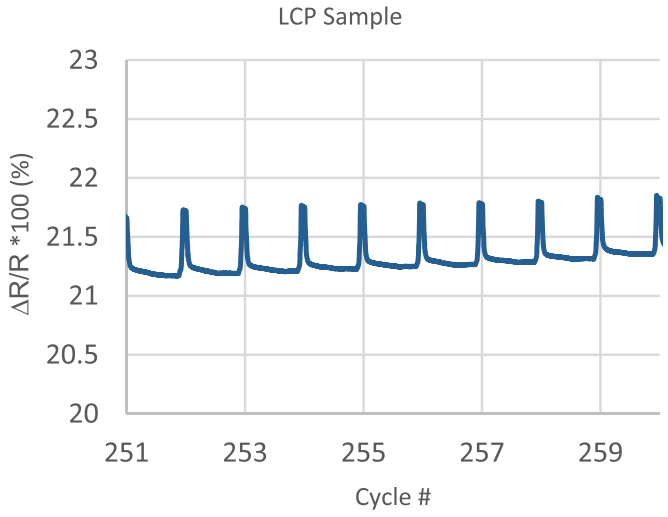

Figure 20. Resistance results of LCP sample just after 250 cycles.

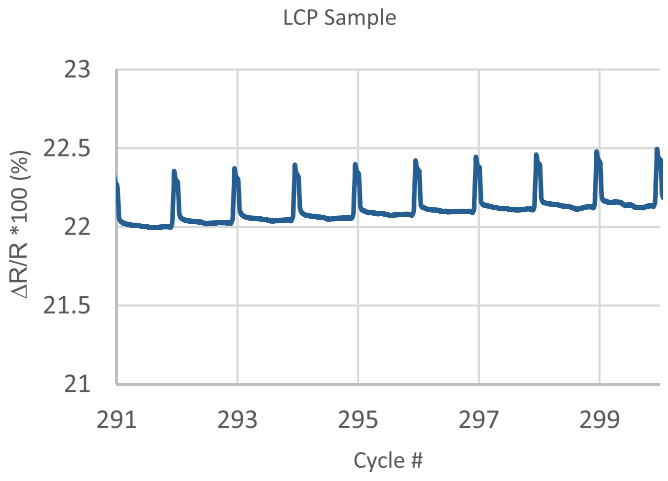

Figure 21. Resistance results of LCP sample at end of test.

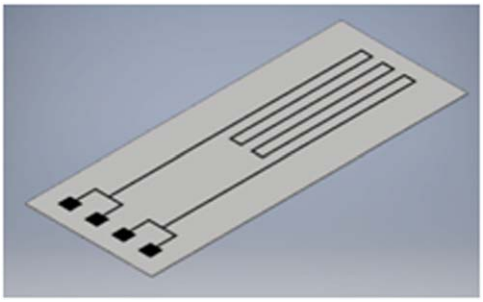

Figure 22. CAD model of Suntronic™ ink serpentine pattern on LCP.

Table 3. Material properties.

Material	Modulus (GPa)	Poisson's Ratio
Rogers Ultralam® 3850 LCP	3.4	0.30
Suntronic™ silver ink	13.5	0.37
Rigid fixtures	200.0	0.30

extremely rigid with a modulus of elasticity of 200 GPa so that the stiffness would be much greater than the silver ink and LCP and the deformation of the fixtures would be negligible. Table 3 shows a summary of the material models used.

3.2. Geometric modeling

3D geometry models for the printed ink on LCP were created in Autodesk® Inventor. The ink structure in figure 23 is 8 μm thick to represent the thickness of four ink layers after curing in the oven. The substrate was modeled as a 50 $\times$ 20 mm rectangle 117.8 μm (7 mils) thick. Figure 22 shows a CAD model of the entire ink and substrate geometry, while figure 23 shows a close-up side view.

To apply the desired deformations to the structure and simulate the actual test conditions, simplified models of the saddle-like and dome fixtures were used. 0.254 mm (0.01 in.) thick sections of the curved areas of the fixtures were created for the simulations. These sections were trimmed to be only as large as the area of the substrate that they were being used to deform. This was done to minimize the number of elements used in the simulations. The sample was placed in between these top and bottom fixtures. The fixtures were placed at a height where they were slightly above and below the sample. Figure 24 shows an example of the LCP sample with saddle-like fixtures.

The printed sample was meshed with 20-node 3D brick elements for the ink structure and 4-node shell elements for the substrate. The fixture was also meshed with 20-node 3D brick elements. A sweep meshing method was used and the ink structure was meshed three layers thick. Fully bonded contact elements were used between the ink and the substrate. In other words, the ink was assumed to be fully bonded to the underlying substrate. Also, three frictionless contact element sets were used between: bottom of substrate to bottom fixture, top of substrate to top fixture, and top of ink to top fixture. These contact elements were present to ensure that the substrate or ink would not penetrate the rigid fixtures or vice versa. Figure 25 shows the mesh of the LCP sample with the saddle-like fixtures.

3.3. Boundary conditions

Conforming the sample to the desired shape was obtained by moving the top fixture downwards toward the bottom fixture and sandwiching the sample. This method of applying the deformation simulates the actual physical test loading. The nodes along the bottom surface of the bottom fixture were fixed in place while the nodes on the bottom surface of the top fixture (inside) were given displacements downwards. Multiple load steps were used with each one displacing the top fixture 0.1 mm. The total vertical displacement was equal to the initial spacing between the fixtures minus the thickness of the ink and substrate. In order to keep the sample from sliding out from in between the fixtures or rotating, two nodes along one of the sides were given in plane displacements of zero while being free to move vertically. Figure 26 shows the geometry of the sample with saddle-like fixtures and the boundary conditions. In figure 26, A is the fixed nodes on the bottom side of the bottom fixture, B is the group of nodes that is only allowed to move vertically to prevent sample sliding, and C is the group of nodes on the bottom side of the top fixture that is displaced downwards.

3.4. Simulation results

The ink structure's X (length) normal strains (ε_{xx}) are shown in figure 27 and the Y (width) normal strains (ε_{yy}) are shown in figure 28 below for the dome bend.

The ink structure's X (length) normal strains (ε_{xx}) are shown in figure 29 and the Y (width) normal strains (ε_{yy}) are shown in figure 30 below for the saddle-like bend.

The maximum principal and maximum shear stresses can be examined to predict the direction of the cracks that develop during cyclic deformation. These stress values were extracted at the same locations where SEM images were taken on the physical samples. The elements used at the corner and side locations of the ink structure are shown in figures 31 and 32.

The theoretical strains in the ink structure can be calculated using (1) and (2) below. The x direction represents the lengthwise direction and y represents the width direction

$$\varepsilon_{xx} = \frac{d}{\rho_x} - \nu\frac{d}{\rho_y}, \tag{1}$$

$$\varepsilon_{yy} = \frac{d}{\rho_y} - \nu\frac{d}{\rho_x}, \tag{2}$$

where d is the distance from the neutral axis, ρ_x is the radius of curvature in the length direction, ρ_y is the

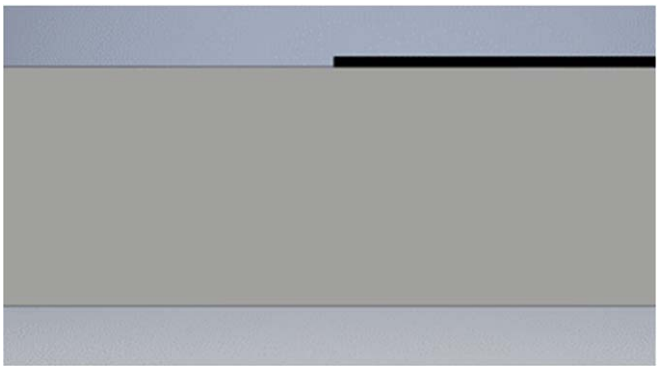

Figure 23. Close-up side view of CAD model Suntronic™ ink on LCP.

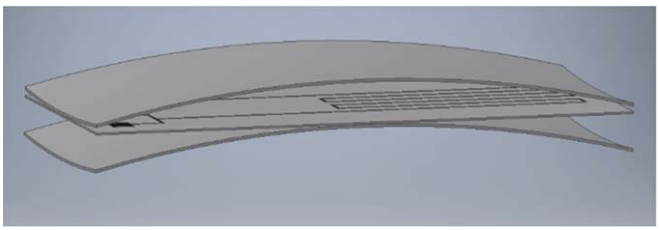

Figure 24. CAD model of LCP sample with saddle-like fixtures.

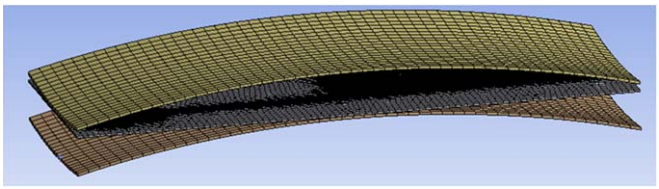

Figure 25. Finite-Element Mesh of LCP Substrate with Printed Ink Placed in between Fixtures.

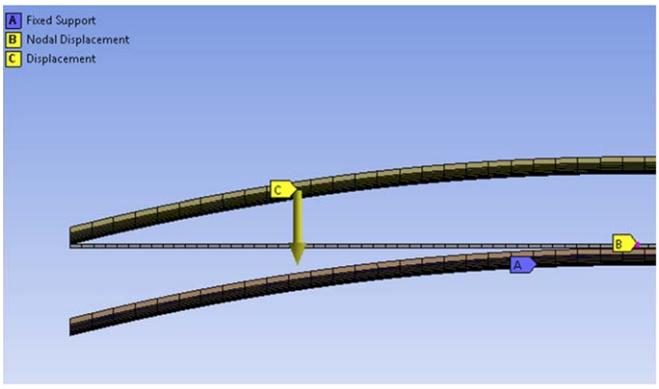

Figure 26. Saddle-like simulation boundary conditions.

radius of curvature in the width direction, and ν is the Poisson's ratio. The theoretical strains for the saddle and dome shapes simulated are shown in table 4.

The length and width strains in the dome simulations, about 0.100%, appear to be higher than the theoretical strains. One possible reason for this is that

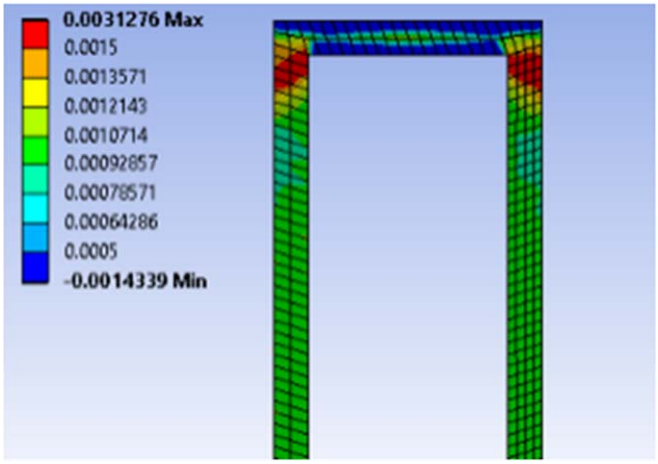

Figure 27. Ink structure length direction normal strain (ε_{xx}) contours in dome fixtures.

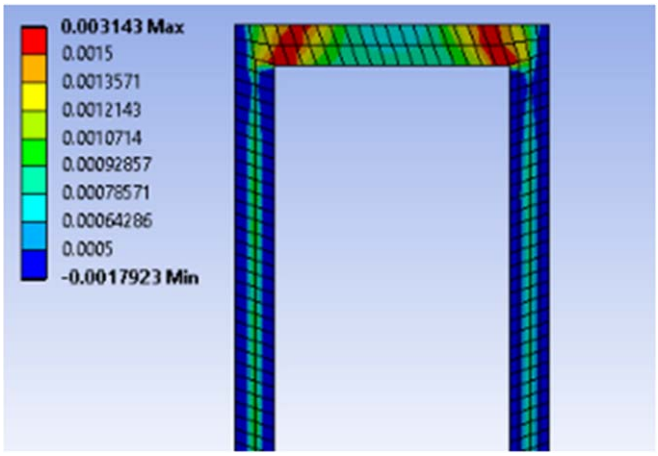

Figure 28. Ink structure width direction normal strain (ε_{yy}) contours in dome fixtures.

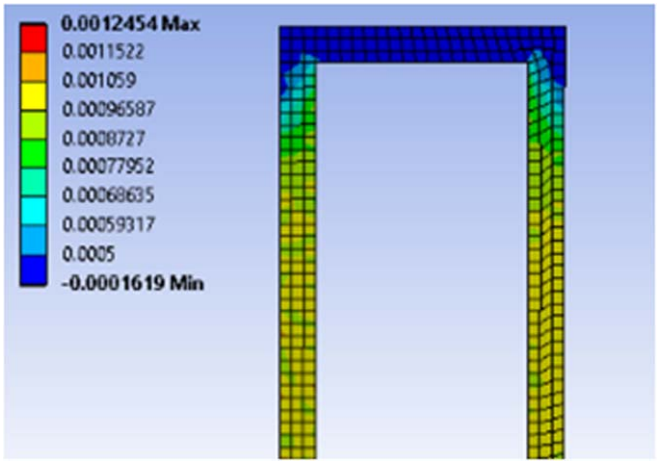

Figure 29. Ink structure length direction normal strain (ε_{xx}) contours in saddle-like fixtures.

the out-of-plane (z axis) compression of the silver ink by the top fixture is not taken into consideration in the analytical formulation. Figure 33 shows the out-of-plane strain (ε_{zz}) of the silver ink and figure 34 shows the length-wise normal (ε_{xx}). Strain, and it is seen that their magnitudes are very close to each other. As seen, the negative strain in the out of plane direction appears to be of the same order of

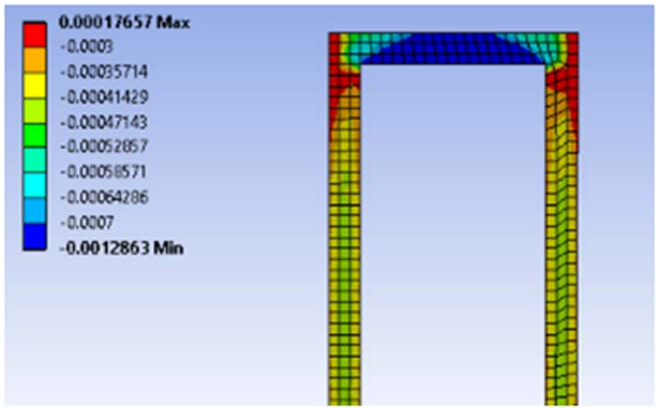

Figure 30. Ink structure width direction normal strain (ε_{yy}) contours in saddle-like fixtures.

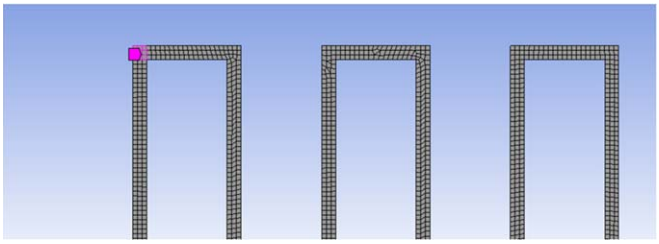

Figure 31. SEM corner location elements.

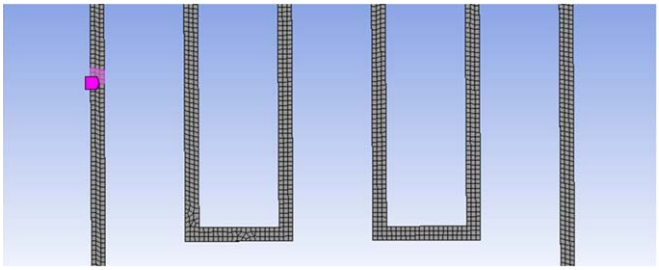

Figure 32. SEM side location elements.

magnitude as the tensile in-plane strain. The Poisson effect when compressing the ink thus causes an increase in the in-plane strain.

The simulated length and width strains for the saddle-like shape are 0.101% and −0.044% respectively. The length strain matches well with the hand calculation, but the width strain is significantly lower. This could be due to the narrow width of the traces, and the edge effects could dominate.

Figure 35 shows the maximum principal stress plot at the corner location next to the SEM imaged cracks at 300 cycles for the long test LCP sample in the saddle-like fixture. As expected, the cracks occur in locations where the stresses are maximum.

Likewise, the maximum principal and shear stress plots with the cracks at the side location at 300 cycles are shown in figure 36.

Table 4. Theoretical strain of printed silver ink on LCP.

Deformation Shape	ε_{xx} (%)	ε_{yy} (%)
4 in. dome	0.0489	0.0489
4 in. saddle-like	0.106	−0.106

At the side location, the cracks appear to be propagating perpendicular to the trace direction. This is expected due to the trace experiencing tension along its length direction and compression in the width direction.

4. Summary

Additive 3D printing can be utilized to quickly fabricate fixtures with many different complex

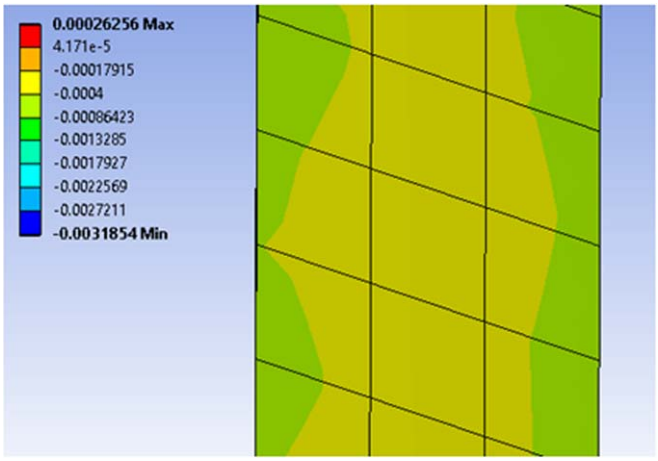

Figure 33. Out of plane strain (ε_{zz}) in the ink structure during dome bend.

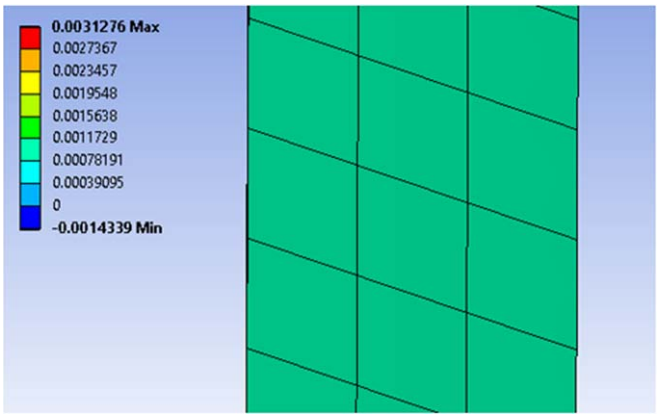

Figure 34. Strain in the length direction (ε_{xx}) of the ink structure during dome bend.

Table 5. Testing summary.

Sample	Number of cycles tested	% Final change in resistance	Cracks observed?
Suntronic™ ink on LCP	300	22.16	Yes
Novacentrix® ink on PET air-dried	50 and 100	−0.24 (50 cycles sample) and 0.78 (100 cycle sample)	Yes (100 cycles sample)
Novacentrix® ink on PET oven-cured	100	−0.69	No

surfaces to use in testing flexible electronics. These fixtures can easily be adapted to fit a UTM and test many different flexible electronics all on the same test apparatus. With appropriate access to the contact pads, various electrical characteristics of the flexible electronic samples can be assessed. A downside of the discussed test is that the fixtures need to be fabricated, and the fabrication can be time consuming and expensive if one needs to test on many different surfaces. Also, the samples undergo mostly bending and very little stretching during testing. Another test that can be used for biaxial stretching is the Bladder Inflation Stretch test [24, 25]. This other test has been demonstrated and is being further developed.

5. Conclusion

A summary of the testing with number of cycles, percent change in resistance at end of test, and whether or not cracks were observed is shown in table 5.

Novacentrix® Metalon® JS-B25P air-dried silver ink serpentine patterns on PET were tested on a dome structure. As the ink structure was put in tension, the resistance increased and then decreased when the structure

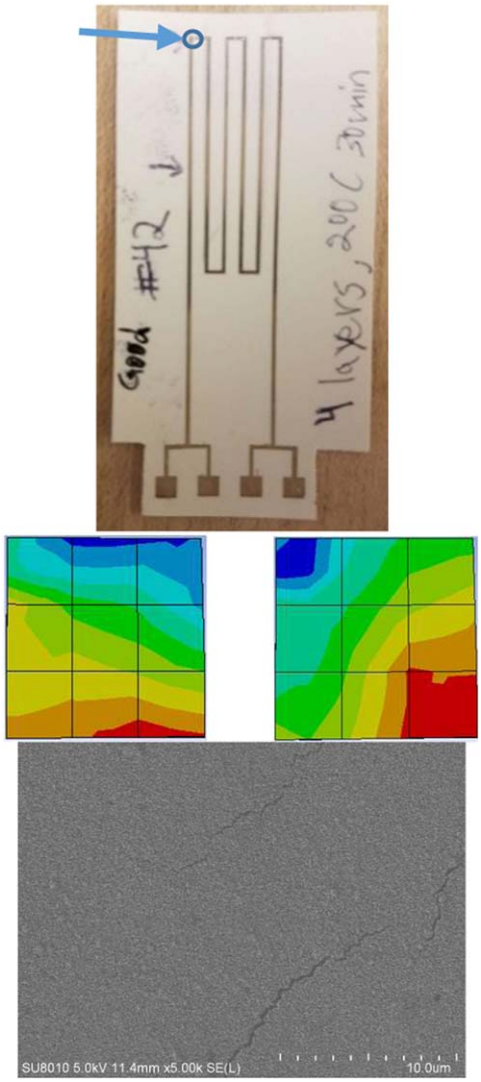

Figure 35. SEM corner locion on sample (top), maximum principal stress (middle left), maximum shear stress (middle right), and cracks at 300 cycles (bottom).

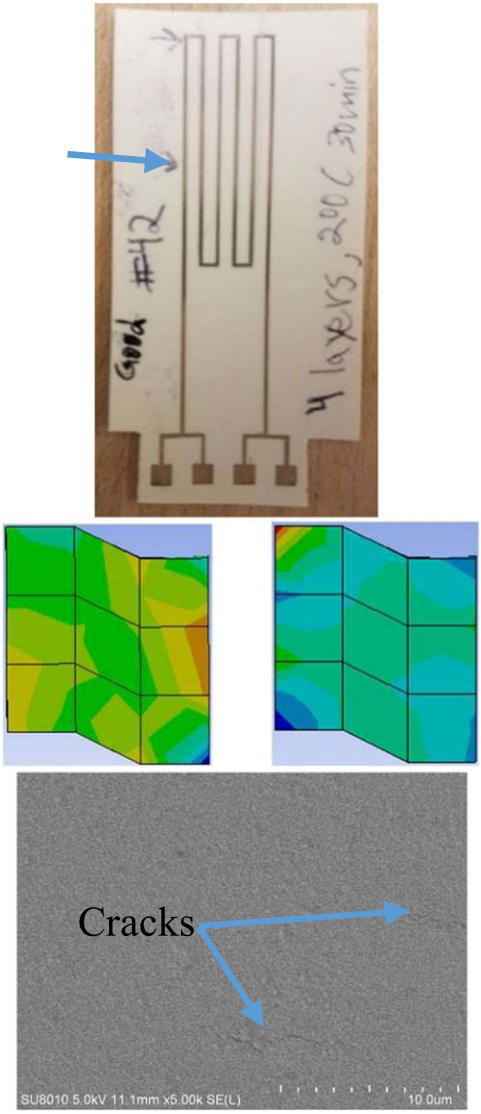

Figure 36. SEM side location on sample (top), maximum principal stress (middle left), maximum shear stress (middle right), and cracks at 300 cycles (bottom).

returned to its original shape. The resistance of the ink pattern decreased for about 50 cycles, and then increased from about 50–100 cycles. Significant interparticle cracking in the printed ink was observed in SEM images. This cracking is believed to be the reason for the increase in resistance. The initial decrease in resistance with cycling is believed to be from the particles rubbing together during as the structure is strained. As the particles rub together, the capping agent on the individual particles is further removed, increasing the electrical contact between the particles. As long as no significant cracking is present, this rubbing together of the particles causes the resistance to decrease.

Novacentrix® Metalon® JS-B25P silver ink serpentine patterns on PET sintered at 90 C for 30 min were also tested on a dome structure. The initial resistance of the silver ink was around half that of the air-dried silver ink on PET. The resistance increased when put into tension and decreased when returned to its original shape. Similar to the air-dried silver ink patterns on PET, the resistance trended downward during repetitive cycling. The oven-sintered silver ink on PET trended downward for all 100 cycles. There were not any visible cracks in the SEM images of the silver structure. The lack of cracking explains the lack of resistance increase during cyclic loading. The decrease of resistance during testing is believed to be caused by the same mechanism as with the air-dried PET samples.

A third set of serpentine patterns was fabricated by printing Sun Chemical® Suntronic™ EMD 5730 silver ink on LCP and curing in an oven at 200 °C. This ink had an average resistance of 24.55 Ω, significantly lower than the other two ink categories. The average resistivity of the ink was 2.72×10^{-7} Ω m. This sample was subjected to a saddle-like bend test. The resistance of the ink increased when conformed to the surface and decreased when returned to its original flat shape. The resistance of the ink increased for all 300 cycles it was subjected to. After 300 cycles, the resistance had increased by over 20%. The lack

of a resistance decrease like that seen from the PET samples is believed to be due to more densification from the higher curing temperature and the lack of a microporous coating on the LCP. The silver ink structure was imaged at 0, 100, 200, 250, and 300 cycles. Cracks were first observed at the corner location at 200 cycles and the side location at 250 cycles. The cracks in the corner location prorogated at an angle of approximately 45° while those in the side location propagated horizontally.

A finite element model was created of the printed Suntronic™ ink on LCP to determine the stress and strain distributions when conformed to the dome and saddle-like surfaces. The max principal and max shear stress contours were observed at the side and corner locations of the geometry where the SEM images were taken on the physical sample. It was observed that the cracks seen in the physical sample were perpendicular to the max principal stress and parallel to the max shear stress contours seen in the finite element simulations. This shows that these simulations can be used to predict the directions in which the fatigue cracks will propagate.

Acknowledgments

This paper is based, in part, on research sponsored by Air Force Research Laboratory under agreement number FA8650-15-2-5401, as conducted through the flexible hybrid electronics manufacturing innovation institute, NextFlex. The U.S. Government is authorized to reproduce and distribute reprints for Governmental purposes notwithstanding any copyright notation, thereon. The views and conclusions contained herein are those of the authors and should not be interpreted as necessarily representing the official policies or endorsements, either expressed or implied, of Air Force Research Laboratory or the U.S. Government.

ORCID iDs

Isaac A Bower https://orcid.org/0000-0002-6054-8428

References

[1] Sillanpää H, Halonen E, Liimatta T and Mäntysalo M 2014 Inkjet printed wireless biosensors on stretchable substrate *2014 Int. Conf. on Electronics Packaging* (Piscataway, NJ: IEEE) (https://doi.org/10.1109/ICEP.2014.6826704)

[2] Kim D-H, Ghaffari R, Lu N and Rogers J A 2012 Flexible and stretchable electronics for biointegrated devices *Annu. Rev. Biomed. Eng.* **14** 113–28

[3] Kim S and Tentzeris M M 2018 Parylene coated waterproof washable inkjet-printed dual-band antenna on paper substrate *Int. J. Microw. Wirel. Technol.* **10** 814–8

[4] Cook B S and Tentzeris M M 2013 A miniaturized wearable high gain and wideband inkjet-printed AMC antenna *2013 IEEE Antennas and Propagation Society Int. Symp. (APSURSI)* (Piscataway, NJ: IEEE) (https://doi.org/10.1109/APS.2013.6710998)

[5] Li Y, Torah R, Beeby S and Tudor J 2012 An all-inkjet printed flexible capacitor on a textile using a new poly(4-vinylphenol) dielectric ink for wearable applications *SENSORS, 2012 IEEE* (Piscataway, NJ: IEEE) (https://doi.org/10.1109/ICSENS.2012.6411117)

[6] Kim D-H, Kim Y-S, Wu J, Liu Z, Song J, Kim H-S, Huang Y Y, Hwang K-C and Rogers J A 2009 Ultrathin silicon circuits with strain-isolation layers and mesh layouts for high-performance electronics on fabric, vinyl, leather, and paper *Adv. Mater.* **21** 3703–7

[7] Yoshihiro K, Hodges S, Cook B S, Zhang C and Abowd G D 2013 Instant inkjet circuits: lab-based inkjet printing to support rapid prototyping of UbiComp devices *2013 ACM Int. Joint Conf. on Pervasive and Ubiquitous Computing* (Zurich: ACM)

[8] DuPont 2011 *DuPont Kapton HN* (https://www.dupont.com/products/kapton-hn.html)

[9] Wypych G 2016 PET poly(ethylene terephthalate) *Handbook of Polymers* (Toronto: ChemTec Publishing) pp 398–403

[10] Fjelstad J and Mahnke D B 2011 Flexible circuit materials *Flexible Circuit Technology* ed D Neer (Seaside, OR: BR Publishing) pp 126–66

[11] Lim J, Kim Jihoon, Young J Y, Kim H, Yoon H G, Lee S-N and Kim Jonghee 2012 All-inkjet-printed metal–insulator–metal (MIM) capacitor *Curr. Appl Phys.* **12** e14–7

[12] Gaikwad A M, Steingart D A, Ng T N, Schwartz D E and Whiting G L 2013 A flexible high potential printed battery for powering printed electronics *Appl. Phys. Lett.* **102** 233302

[13] Lee S-Y 2017 Beyond flexible batteries: aesthetically versatile, printed rechargeable power sources for smart electronics *SPIE Defense+Security (Anaheim, California)* (SPIE)

[14] Chow J H, Sitaraman S K, May C and May J 2018 Study of wearables with embedded electronics through experiments and simulations *2018 IEEE 68th Electronic Components and Technology Conf. (ECTC)* (Piscataway, NJ: IEEE) (https://doi.org/10.1109/ECTC.2018.00126)

[15] Sim G-D, Hwangbo Y, Kim H-H, Lee S-B and Vlassak J J 2012 Fatigue of polymer-supported Ag thin films *Scr. Mater.* **66** 915–8

[16] Torres Arango M A, Cokeley A M, Beard J J and Sierros K A 2015 Direct writing and electro-mechanical characterization of Ag micro-patterns on polymer substrates for flexible electronics *Thin Solid Films* **596** 167–73

[17] Chen R, Chow J, Taylor C, Meth J and Sitaraman S K 2018 Adaptive curvature flexure test to assess flexible electronic systems *2018 IEEE 68th Electronic Components and Technology Conf. (ECTC)* (Piscataway, NJ: IEEE) (https://doi.org/10.1109/ECTC.2018.00044)

[18] Halonen E, Halm A, Karinsalo T, Iso-Ketola P, Mäntysalo M and Mäkinen R 2012 Dynamic bending test analysis of inkjet-printed conductors on flexible substrates *2012 IEEE 62nd Electronic Components and Technology Conf. (ECTC)* (Piscataway, NJ: IEEE) (https://doi.org/10.1109/ECTC.2012.6248810)

[19] Li H U and Jackson T N 2016 Flexibility testing strategies and apparatus for flexible electronics *IEEE Trans. Electron Devices* **63** 1934–9

[20] ASTM 2016 ASTM F2750 - 16: Standard Test Method for Determining the Effects of Bending a Membrane Switch or Printed Electronic Device

[21] Glushko O and Cordill M J 2014 Electrical resistance decrease due to grain coarsening under cyclic deformation *J. Minerals, Metals Mater. Soc. (TMS)* **66** 598–601

[22] Glushko O, Klug A, List-Kratochvil E J W and Cordill M J 2016 Relationship between mechanical damage and electrical degradation in polymer-supported metal films subjected to cyclic loading *Mater. Sci. & Eng.* A **662** 157–61

[23] Rogers Corporation 2016 *Ultralam 3850HT Liquid Crystalline Polymer Circuit Material Double-Clad Laminates*

[24] Stewart B G, Bower I and Sitaraman S K 2019 Bladder inflation method for mechanical testing of stretchable electronics and wearable devices *IPC APEX EXPO 2019, Jan 29-31* (San Diego, CA: IPC)

[25] Stewart B G and Sitaraman S K 2019 Bladder inflation stretch test method for reliability characterization of wearable electronics *2019 IEEE 69th Electronic Components and Technology Conf.* 28–31 May (Piscataway, NJ: IEEE) (https://doi.org/10.1109/ECTC.2019.00065)